

Improved Ferrite Number Prediction in Stainless Steel Arc Welds Using Artificial Neural Networks — Part 2: Neural Network Results

A new neural network model predicts Ferrite Number with significantly more accuracy than existing constitution diagrams

BY J. M. VITEK, Y. S. ISKANDER AND E. M. OBLow

ABSTRACT. The development of a neural network model, named FNN-1999, for predicting Ferrite Number in arc welds as a function of alloy composition is described in Part 1. In this paper, the results of the model are compared to other means of predicting Ferrite Number in stainless steel welds. It was found the accuracy of the FNN-1999 model in predicting Ferrite Number is superior to that of the WRC-1992 diagram, the Function Fit model and a preliminary neural network model developed earlier. The error in fitting the current model to the training set was 40% less than that for the WRC-1992 diagram. In addition, the FNN-1999 model removes the restriction found in WRC-1992 and many other constitution diagrams that each element's contribution to the Ferrite Number is constant, regardless of the overall composition. Examples are given that show that with this added flexibility of the FNN-1999 model, the impact of alloying additions varies as a function of concentration, and in some cases the variation can be quite significant.

Introduction

The ability to predict the ferrite content in stainless steel arc welds is essential, as described in detail in Part 1 (Ref. 1). Although currently available constitution diagrams are reasonably accurate in predicting Ferrite Number, improved accuracy and flexibility that takes the alloy composition into account is desir-

able (Ref. 1). Neural network models are ideally suited for predicting Ferrite Number in welds because of their flexibility and their ability to account for nonlinear behavior. In Part 1 of this paper (Ref. 1), the development of a neural network model (FNN-1999) for predicting Ferrite Number is described in detail, including the basic principles behind neural networks, the identification of the optimum network architecture and the specifications of the network weights for a "best" network for ferrite prediction. Here, in Part 2, the neural network model results are presented, including an assessment of the prediction accuracy compared with other available methods. Calculations are also presented that show composition-dependent effects of various elements and the ability of the neural network model to capture these effects when making ferrite predictions.

Optimum Neural Network Model

An optimum neural network architecture was identified in Part 1 and is shown in Fig. 1. The network consists of thirteen

input nodes, corresponding to the compositions of thirteen alloying elements (C, Cr, Ni, Mo, N, Mn, Si, Fe, Cu, Ti, Nb, V and Co), six hidden nodes and one output node (Ferrite Number). The network was trained on the same extensive data set (Refs. 2–4) ("complete training data set") used to establish the WRC-1992 constitution diagram (Ref. 5). Details regarding the development of the network are provided in Part 1 (Ref. 1). The best network is defined by a series of coefficients (weights) that correspond to the node connections in Fig. 1 (these are also given in Part 1). The range of alloying element concentrations over which the network is applied is given in Table 1. As described in detail in Part 1, non-zero concentrations must be used for eight of the elements (C, Cr, Ni, Mo, N, Mn, Si, Fe). For the remaining five elements (Cu, Ti, Nb, V, Co), a zero concentration is appropriate when chemical analysis results are not available. Some results are also presented that consider another data set (Refs. 6, 7) ("supplemental data set"). These data were not used in the training of any of the predictive models and therefore this data set represents an independent set of experimental results useful for evaluating the prediction accuracy, although the composition range it covers is more limited than the training data set (Table 1).

Results and Discussion

Prediction Comparisons of Various Models

Ferrite Number (FN) was calculated using the neural network for all alloy compositions in the data set used for training the neural network, and the predicted FN values are plotted against ex-

KEY WORDS

Ferrite Number
Constitution Diagram
Neural Network
WRC-1992
Stainless Steel

J. M. VITEK and E. M. OBLow are with Oak Ridge National Laboratory, Oak Ridge, Tenn. Y. S. ISKANDER is a graduate student at the Georgia Institute of Technology, Atlanta, GA.

Table 1 — Ranges in Composition and FN for the Training and Supplemental Data Sets

	C	Cr	Ni	Mo	N	Mn	Fe	Si	Cu	Ti	Nb	V	Co	FN
Complete Training Data Set														
Min.	0.008	14.74	4.61	0.01	0.01	0.35	45.60	0.03	0.0	0.0	0.0	0.0	0.0	0
Max.	0.2	32	33.5	6.85	0.3	12.67	72.51	1.3	3.04	0.54	0.88	0.23	0.32	117
Supplemental Data Set														
Min.	0.013	16.25	8.4	0.0	0.018	0.1	56.42	0.21	0.0	0.0	0.0	0.0	0.0	0
Max.	0.13	23.91	13	2.86	0.12	9.5	72.39	1.64	0.0	0.0	0.78	0.0	0.0	30.1

Table 2 — Comparison of Errors (experimental — predicted FN) for the FNN-1999 Model and the WRC-1992 Constitution Diagram (Ref. 5) (Training Data Set)

Absolute Error	FNN-1999 Model		WRC-1992 Constitution Diagram	
	Number of Points	% of Total	Number of Points	% of Total
Entire Training Data Set (961 data points)				
≤ 1.5	621	64.6	531	55.3
≤ 2.5	764	79.5	721	75.0
≤ 3.5	826	86.0	794	82.6
≥ 9.5	32	3.3	56	5.8
Subset of Training Data Set with FN ≤ 30 (828 data points)				
≤ 1.5	599	72.3	516	62.3
≤ 2.5	733	88.5	696	84.1
≤ 3.5	780	94.2	761	91.9
≥ 9.5	4	0.5	14	1.7
Subset of Training Data Set with FN ≤ 18 (797 data points)				
≤ 1.5	590	74.0	509	63.9
≤ 2.5	722	90.6	679	85.2
≤ 3.5	763	95.7	741	93.0
≥ 9.5	3	0.4	13	1.6

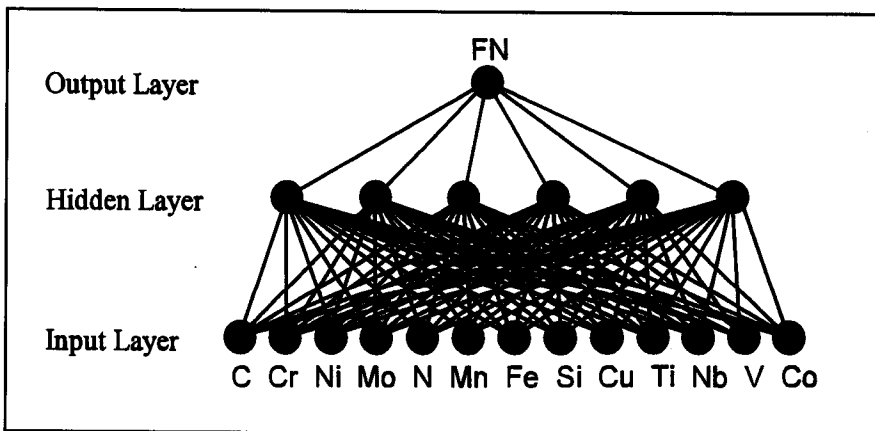


Fig. 1 — Optimum neural network for predicting Ferrite Number as a function of composition, as developed in Part 1 (Ref. 1).

perimental measurements in Fig. 2A. The same data were used to establish other predictive models. For comparison with Fig. 2A, similar plots of predicted vs. experimentally measured FN are shown in Fig. 2 B, C and D using the WRC-1992 constitution diagram (Ref. 5), the Function Fit model (Ref. 8) and the earlier, more limited, eight-element neural network model (Ref. 9), respectively. The straight lines represent exact agreement

between the predicted and measured FN values. The WRC-1992 predictions for the data were calculated using an interpolation program based on the published diagram (Ref. 10). It can be seen immediately that all four models do a very respectable job of predicting FN over the entire range of FN for most of the data. However, there are numerous data points that deviate considerably from the line of perfect fit in Fig. 2 B, C and D. In partic-

ular, in the range of experimental FN of 0 to 10, the WRC-1992 model (Fig. 2B) often predicts FN values in excess of 20. In addition, at higher FN values, all three earlier models have the potential for errors in excess of 20 FN, and in some cases the difference between predicted and experimental FN is more than 40 FN. These errors appear as both overestimates and underestimates. The new neural network FNN-1999 model results in Fig. 2A show a dramatically reduced tendency for large errors, both at low and high FN levels.

A more quantitative comparison can be made by examining the error distributions for the different models. Such a comparison between the FNN-1999 model and the WRC-1992 constitution diagram is shown in Fig. 3. It is quite clear that most of the data are fit very well by either model, with an absolute error of less than 3 FN in most cases. In addition, the error distributions for both models are symmetrical about 0, indicating the model fits are correct. However, it is also clear from Fig. 3 the tails of the error distributions are significantly greater for the WRC-1992 predictions, indicating there are considerably more large errors for that model. The error distributions are quantified in Table 2. Along with comparing errors over the entire training data set, errors are compared in Table 2 over more restricted ranges of FN, namely for FN ≤ 30 and for FN ≤ 18. These limited ranges in FN have been used in the past for evaluating the accuracy of predictive models (Refs. 5, 6, 8). In all of the comparisons in Table 2, the FNN-1999 model is noticeably better than the WRC-1992 constitution diagram. In some cases, 90% of the data have errors less than 3.5 FN when using the FNN-1999 model. Table 2 also shows the number of large errors in predicted FN is considerably less for the FNN-1999 model. This applies over the entire range of FN as well as for the restricted ranges of FN ≤ 18 or FN ≤ 30. For the entire data set, the number of prediction errors ≥ 9.5 is cut nearly in half by the FNN-1999 model. For the restricted ranges of FN, the number of prediction errors ≥ 9.5 is reduced by approximately 75%.

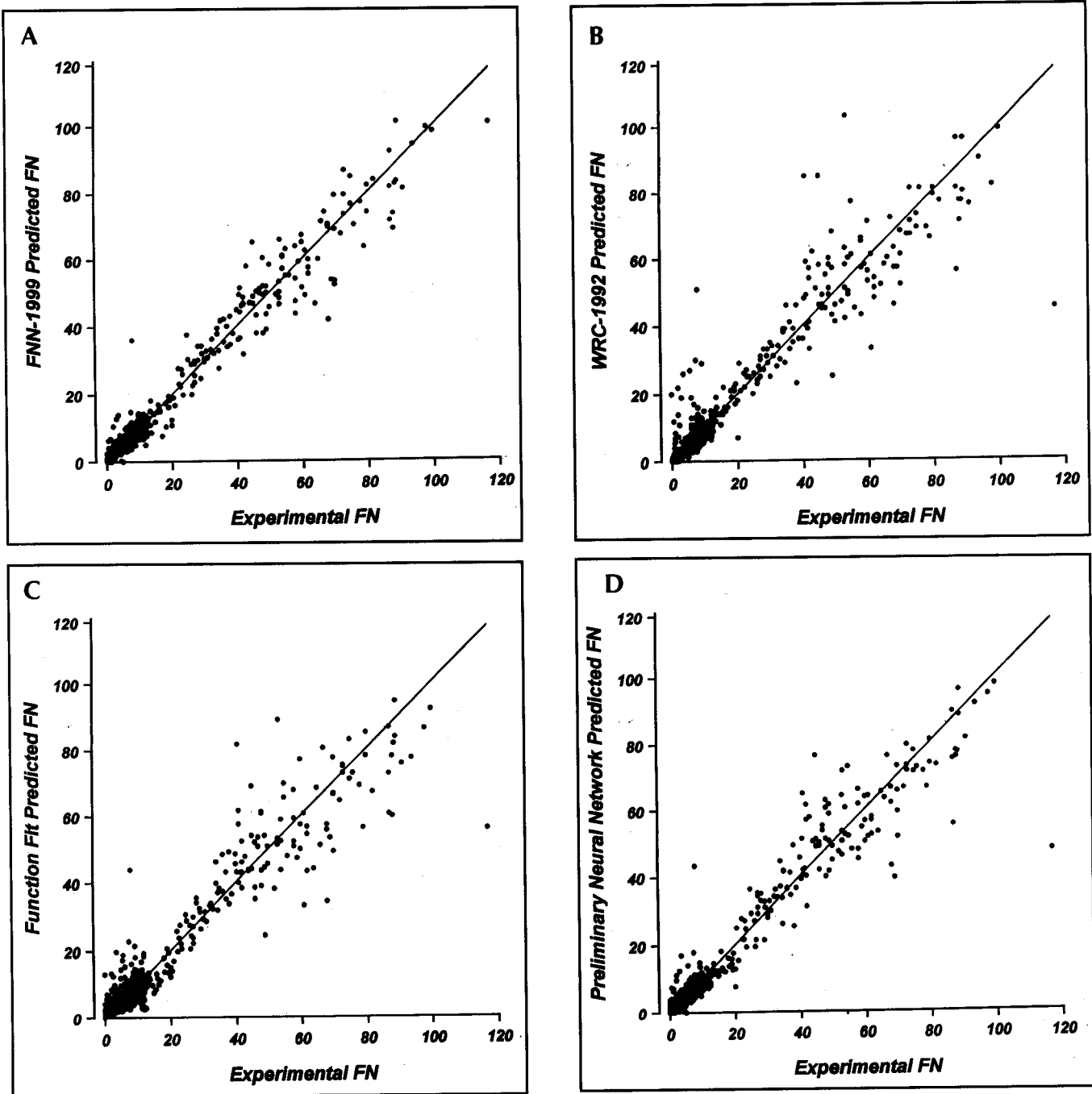


Fig. 2 — Experimentally measured FN vs. predicted FN for the complete training data set for four different predictive models. A — FNN-1999 model from the present study; B — WRC-1992 constitution diagram (Ref. 5); C — Function Fit model (Ref. 8); D — earlier neural network model that considered only eight elements (Ref. 9).

The root mean square (RMS) errors between the measured and predicted FN values for all four FN prediction methods are compared in Table 3. These errors provide a quantitative measure of the degree to which the various models “fit” the complete data set on which they were all trained. While the Function Fit model and WRC-1992 diagram accuracies are comparable, the earlier eight-element neural network model showed a significantly reduced RMS error. The present

neural network model, FNN-1999, with the extension from 8 to 13 elements, has the lowest RMS error of all four models, with a 40% improvement over the WRC-1992 constitution diagram RMS error and a 27% improvement over the earlier neural network model.

When comparing the FNN-1999 model for Ferrite Number prediction with the WRC-1992 diagram, it should be noted the WRC-1992 diagram has a quoted upper limit for the nickel equivalent (Ni_{eq}) of 17. This limit was imposed

due to the scarcity of data for $Ni_{eq} > 17$, but Lake (Ref. 11) has recently shown the WRC-1992 diagram is accurate beyond this limit. No attempt was made in the present study to exclude the experimental data with $Ni_{eq} > 17$ in the training routine. In the entire experimental data set of 961 points, there were 89 measurements on alloy compositions with $Ni_{eq} > 17$. The RMS error of the WRC-1992 predictions for these 89 measurements was cal-

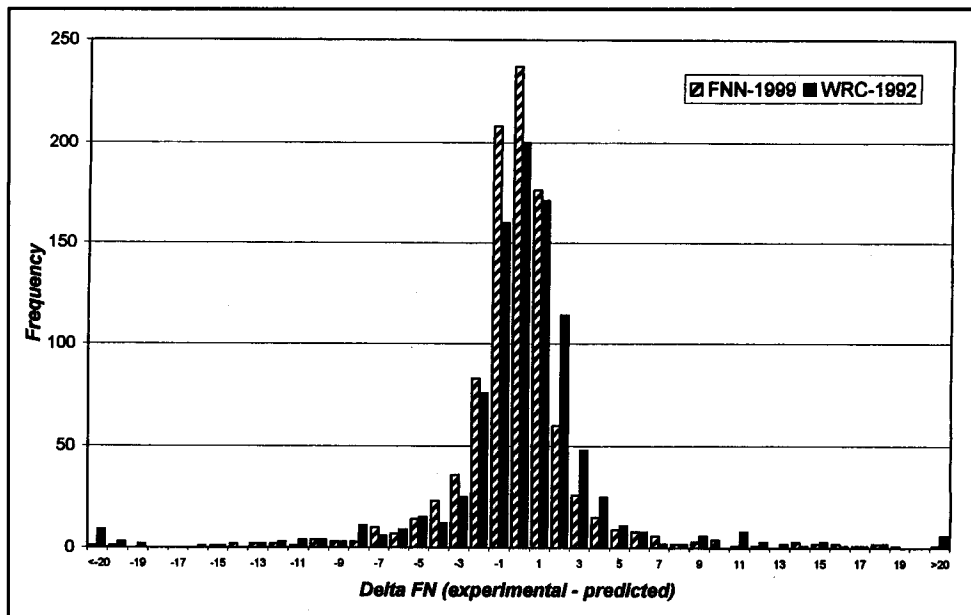


Fig. 3 — Error distributions (experimental FN; predicted FN) for the complete training data set for the FNN-1999 model and the WRC-1992 constitution diagram (Ref. 5).

culated and found to be essentially the same as for the entire data set (5.9 vs. 5.8, respectively). Thus, it was concluded inclusion of all the data when comparing the WRC-1992 predictions with the neural network model did not introduce any significant increase in the calculated errors for WRC-1992.

Of course, the large differences between prediction and experiment may be due to errors in the experimental data. Unfortunately, it is impossible to assess the accuracy of the experimental data at this time. However, occasional large discrepancies in Ferrite Number prediction vs. measurement were also found for the supplemental data set when using the WRC-1992 diagram, as described later. These errors were, once again, considerably reduced with the FNN-1999 model trained on the complete "training set," including any potentially "bad" experimental points. This observation suggests the effect of bad data is small and that the large deviations using the WRC-1992 are real prediction errors that are removed with the FNN-1999 model.

Table 3 — Comparison of Root Mean Square Errors for Complete Training Data Set for Four FN Prediction Methods

Prediction Method	Root Mean Square Error
FNN-1999 Model	3.5
WRC-1992 (Ref. 5)	5.8
Function Fit Model (Ref. 8)	5.6
Earlier Neural Network Model (Ref. 9)	4.8

Model Comparisons Using an Independent Data Set

A second means of assessing the accuracy of the FNN-1999 model compared to other predictive tools is to apply the model to an independent data set. The supplemental data set described earlier was used for this purpose. In a manner similar to Figs. 2 and 3, the predictions for this independent data set are plotted vs. experimentally measured FN in Fig. 4 and the error distributions are shown in Fig. 5. Calculations using the WRC-1992 constitution diagram are also shown in Figs. 4 and 5. From these figures, it is clear both the FNN-1999 model and the WRC-1992 constitution diagram tend to underestimate the FN. The error distributions in Fig. 5 are asymmetrical, being centered about $\Delta FN = 1$. This is an indication the data set had an inherent

bias compared to the data used for training. This may be a result of a bias in the chemical analysis or in the FN measurements themselves. The degree of asymmetry is somewhat less for the neural network model. As was found for the training data set, the WRC-1992 has the potential for larger errors; errors for the WRC-1992 diagram were as large as 14, while the largest error for the FNN-1999 model was only 7.

The errors are quantitatively compared in Table 4. The fraction of the entire data set included within $\Delta FN < 1.5$ and $\Delta FN < 2.5$ is less than that found for the training data set — Table 2. This is a consequence of the fact that the error distribution is not centered about 0 for the supplemental data set calculations. If the scatter is evaluated using $\Delta FN = 1$ as the center (values in parentheses in Table 4) the scatter is comparable to that found in Table 2.

Examination of Table 4 indicates the FNN-1999 model is more accurate than the WRC-1992 constitution diagram in that more data fall within a specified small error limit. When considering the entire supplemental data set, Table 4 also illustrates the tendency for large errors in the WRC-1992 predictions. Table 4 shows comparable trends when the data are restricted to $FN \leq 18$. RMS prediction errors for all four models for the supplemental data set are compared in Table 5. As was true earlier, the FNN-1999 model has the lowest RMS error. In general, the RMS errors are smaller for the supplemental data set than for the training data set (compare Tables 5 and 3). This is most likely due to the fact that the original training data set covered a much broader (higher) range of FN values, and at higher FN levels larger absolute errors were found more frequently.

It is noteworthy the supplemental data

Table 4 — Comparison of Errors (Experimental — Predicted FN) for the FNN-1999 Model and the WRC-1992 Constitution Diagram (Ref. 5) (Supplemental Data Set)

Absolute Error	FNN-1999 Model		WRC-1992 Constitution Diagram	
	Number of Points	% of Total	Number of points	% of Total
Entire Supplemental Data Set (265 data points)				
≤ 1.5	136 (163)	51.3 (61.5)	110 (145)	41.5 (54.7)
≤ 2.5	198 (211)	74.7 (79.6)	189 (210)	71.3 (79.2)
≤ 3.5	230 (240)	86.8 (90.6)	231 (251)	87.2 (94.7)
≥ 9.5	0 (0)	0 (0)	4 (4)	1.5 (1.5)
Subset of Supplemental Data Set with $FN \leq 18$ (254 data points)				
≤ 1.5	133 (166)	52.4 (63.0)	108 (143)	42.5 (56.3)
≤ 2.5	194 (207)	76.4 (81.5)	185 (208)	72.8 (81.9)
≤ 3.5	225 (235)	88.6 (92.5)	227 (246)	89.4 (96.9)
≥ 9.5	0 (0)	0 (0)	0 (0)	0 (0)

Values in parentheses are calculated using $\Delta FN = 1$ as the center of the error distribution.

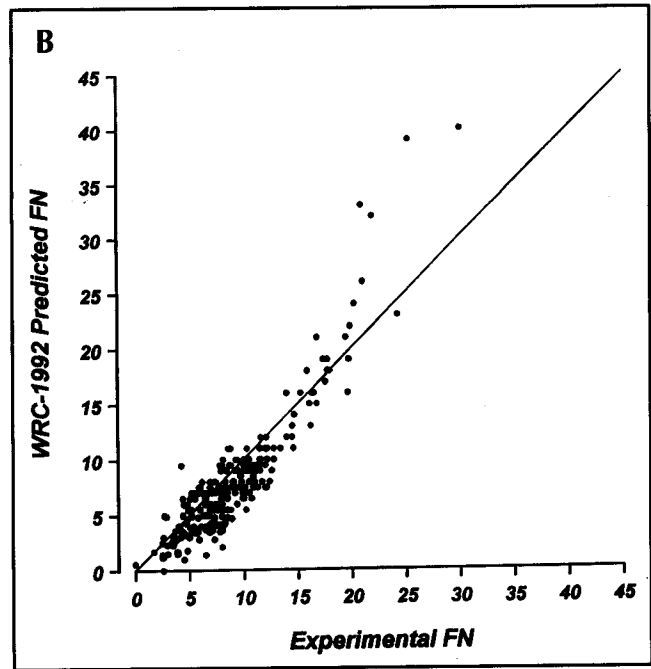
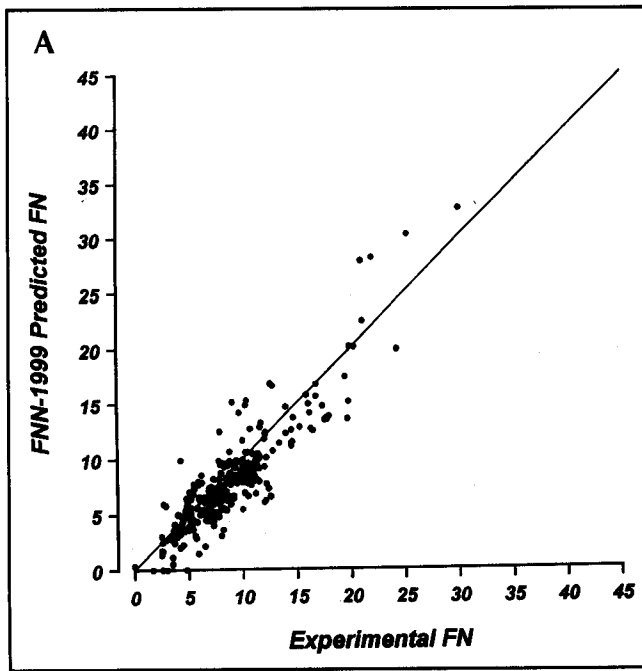


Fig. 4 — Experimentally measured FN vs. predicted FN for the supplemental data set for two different predictive models. A — FNN-1999 model from the present study; B — WRC-1992 constitution diagram (Ref. 5).

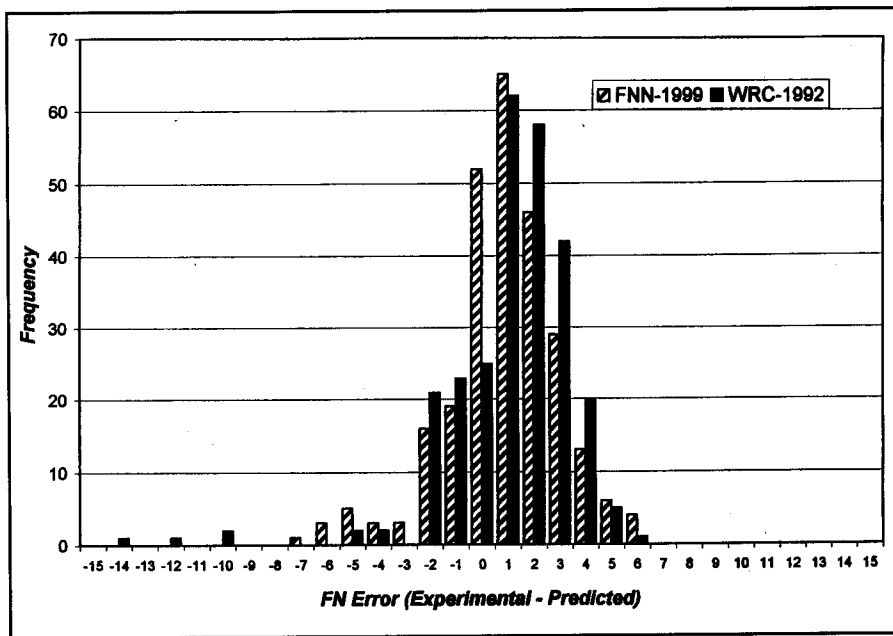


Fig. 5 — Error distribution (experimental FN; predicted FN) for the supplemental data set for the FNN-1999 model and the WRC-1992 constitution diagram (Ref. 5).

Table 5 — Comparison of Root Mean Square Errors for Supplemental Data Set for Four FN Prediction Methods

Prediction Method	Root Mean Square Error
FNN-1999 Model	2.3
WRC-1992 (Ref. 5)	2.6
Function Fit Model (Ref. 8)	5.1
Earlier Neural Network Model (Ref. 9)	2.6

Predictability Evaluation of the FNN-1999

The final method for evaluating the predictability of the neural network was to train the network on an “almost complete” training set, and then test the network on the few data points (~ 1%) left out of the training set. This was done for ten different 99%-1% combinations. This method provides a better indication of the prediction RMS error than that shown in Table 3 since the predictions are for new alloy compositions not used during the training of the network. The RMS errors in Table 3 are an indication of how well the neural network model (or the other models) can be fitted to the data, while the RMS error from the 99%-1% calculations is a true prediction error for the 1% test data that are not used during the network training. The average RMS error for these ten tests was 3.3. This value is comparable to the 3.5 RMS error

set covered a relatively small range in FN. Of the 265 data points, 254 corresponded to $FN \leq 18$. This is the range over which the WRC-1992 diagram was optimized. Therefore, the fact that the FNN-1999

model is more accurate than the WRC-1992 diagram, even in this limited range of FN, is significant, even though the extent of improvement is less than that for the training data set (compare Tables 3 and 5).

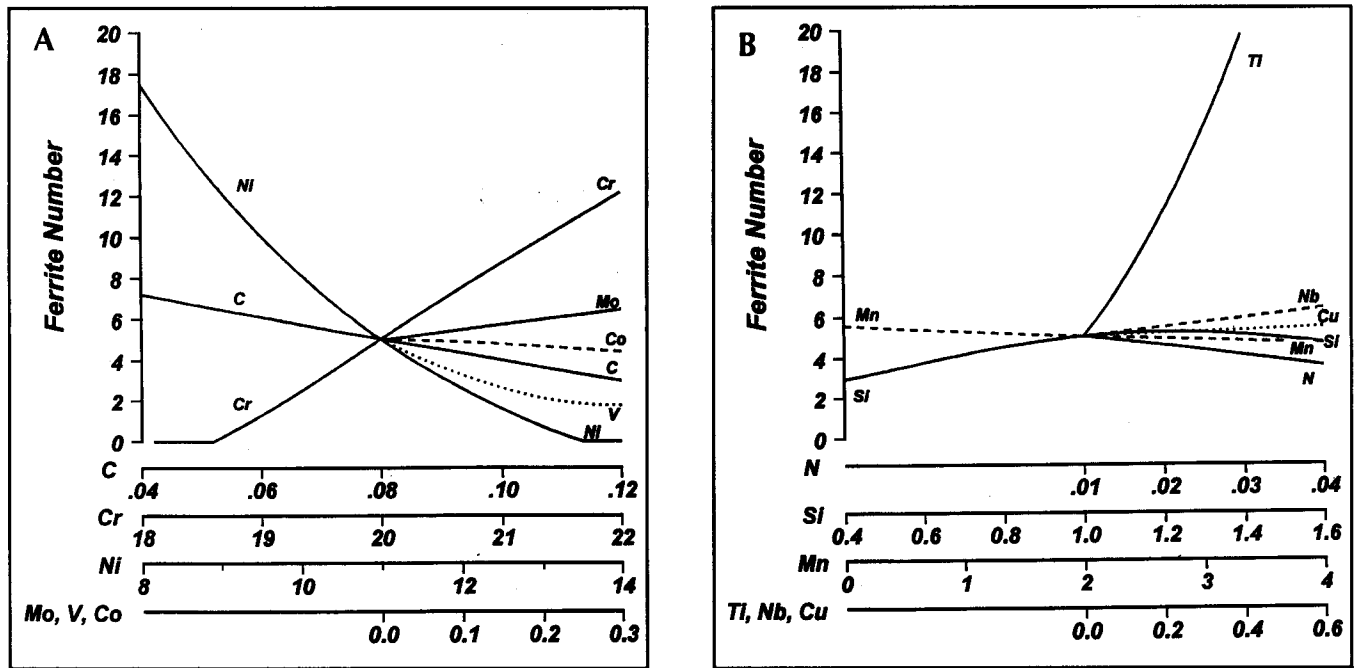


Fig. 6 — Calculated FN vs. concentration for a typical austenitic stainless steel base composition. Calculations were performed using the FNN-1999 model. A — C, Cr, Ni, Mo, V, Co; B — N, Si, Mn, Ti, Nb, Cu. The base metal concentration is 65.9 Fe-20 Cr-11 Ni-0.08 C-0.01 Mo-0.01 N-2 Mn-1 Si. The plots show the difference in FN when one element is varied and all other concentrations are held constant at the base metal value (except Fe, which is adjusted to compensate for the varying element concentration).

Table 6 — Composition Ranges around a Starting Austenitic Stainless Steel Composition for Which FN Was Calculated as a Function of Concentration Using the FNN-1999 Model

	C	Cr	Ni	Mo	N	Mn	Si	Cu	Ti	Nb	V	Co
start	0.08	20	11	0.01	0.01	2	1	0	0	0	0	0
Min.	0.02	18	8	0.01	0.01	0	0.2	0.0	0.0	0.0	0.0	0.0
Max.	0.12	22	14	0.3	0.04	4	1.6	0.6	0.6	0.6	0.3	0.3

found for the complete training data set — Table 3. This indicates the training set errors (Table 3), and presumably the error distribution as well, are representative of the errors that can be expected from independent data. The assessment of predictability with this 99%-1% method has a distinct advantage over the use of the supplemental data set. As seen in Fig. 4, the supplemental data set covers only a limited range in FN, from 0 to 30. Since the neural network model was developed to predict FN over a much broader range in FN (0 to 117), a test over this expanded range is more appropriate. The nature of the 99%-1% test is such that all data can be, in principle, included in the 1% test sets and, therefore, the entire range of FN is tested. The 99%-1% prediction test could not be made for the WRC-1992 diagram, and so a comparison of predictability among the two models using this approach was not possible.

Composition-Dependent Behavior

It would be desirable to interpret the final weight coefficients in the neural network (Tables B-2 and B-3, Appendix B in Part 1) and identify their relationship to the coefficients in the expressions for the chromium equivalent (Cr_{eq}) and Ni_{eq} factors. Unfortunately, a direct interpretation of the neural network weights is not possible. While some hidden nodes are strongly influenced by some elements, with large positive or negative weights for the corresponding input nodes, the contributions from these nodes are then adjusted by the weights from the hidden to the output layer. Therefore, a direct interpretation of the elemental contributions to the final FN is rather difficult, or even impossible. Instead, as described below, the effect of various element additions can be examined by simply calculating the FN as a function of composition.

As noted in Part 1, a severe limitation of the most widely used constitution diagrams is that the coefficients in the terms for the Cr_{eq} and Ni_{eq} factors are constant. This means the influence of a given element on the FN is the same over the entire composition space and is totally independent of any other element concentrations. This is unlikely to be an accurate description of real behavior. This potential limitation is removed with the use of neural networks. Nonlinear effects and element interactions are all possible in the neural network framework. It is valuable to investigate how the elemental contributions vary, if at all, when the overall composition is changed. This was done by specifying a starting base composition and then allowing each element to vary over a limited range, adjusting the Fe concentration accordingly but holding all other element concentrations constant. The first base composition consid-

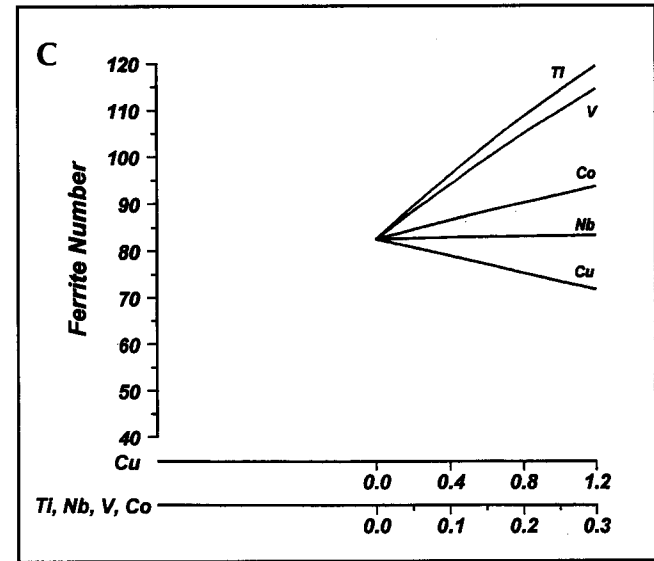
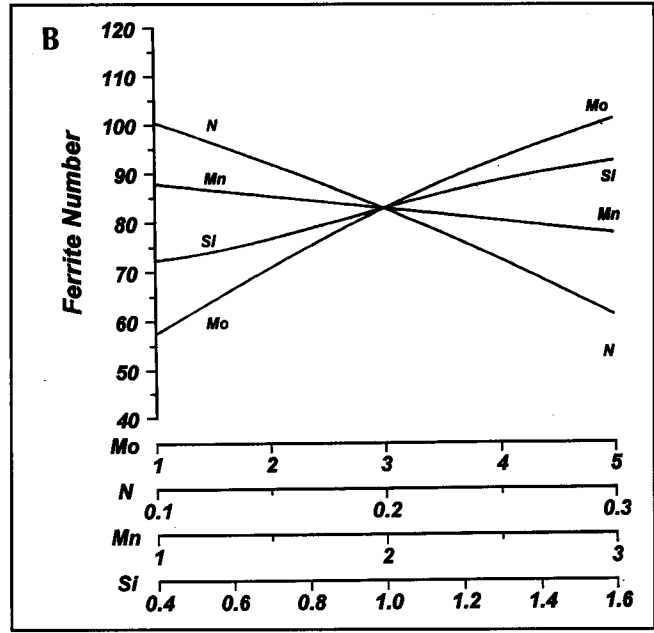
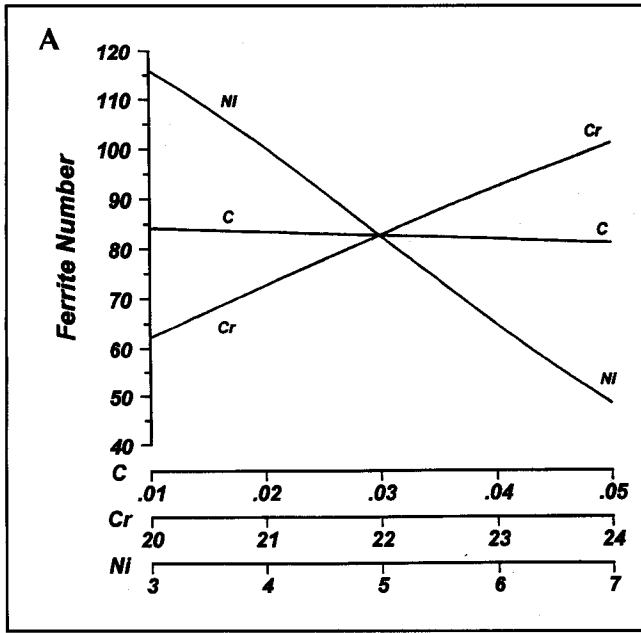


Fig. 7 — Calculated FN vs. concentration for a typical duplex stainless steel base composition. Calculations were performed using the FNN-1999 model. A — C, Cr, Ni; B — Mo, N, Mn, Si; C — Cu, Ti, Nb, V, Co. The base metal concentration is 66.77 Fe-22 Cr-5 Ni-3 Mo-2 Mn-1 Si-0.03 C-0.2 N. The plots show the variation in FN when one element is varied and all other concentrations are held constant at the base metal value (except Fe, which is adjusted to compensate for the varying element concentration).

ered, comparable to a typical austenitic stainless steel, was (in wt-%) 65.9 Fe-20 Cr-11 Ni-0.08 C-0.01 Mo-0.01 N-2 Mn-1 Si. The FN was calculated using the FNN-1999 model for this base composition as well as for a range of concentrations for each of 12 elements (Fe was not considered since it was varied to compensate for the independently varying concentration). The range of values that were examined is listed in Table 6. The calculated FN vs. concentration is plotted in Fig. 6. Note the concentration scale varies according to the element, and only one element concentration is allowed to change at a time, with all other elements (except Fe) held constant at the base metal concentration.

Several features are immediately noticeable in Fig. 6. First, the effect of concentration on FN varies dramatically according to the element that is varied, with some elements increasing the FN as the concentration increases and others showing the opposite effect. It is also clear the change in FN is not necessarily linear with concentration. In particular, a nonlinear variation is found for V and Si, and, to a lesser degree, for Ni and Ti. For the austenitic stainless steel base composition, several elements produce a positive slope for the curves, including Cr, Ti, Mo, Nb and Cu. The elements that result in a negative slope are Ni, V, C, N, Mn and Co. The slope of the FN vs. concentration curve changes from positive to negative for Si. The identification of these trends is extremely valuable, and is totally overlooked by currently available constitution diagrams. The grouping of elements according to the slopes corresponds to the process of grouping elements in the Cr_{eq} and Ni_{eq} expressions.

Various expressions for the Cr_{eq} and Ni_{eq} are available (Refs. 5, 12). In general, some or all of the following elements are included in the Cr_{eq} expressions: Cr, Ti, Mo, Nb, V and Si. Similarly, some or all of the following elements are included in the expressions for the Ni_{eq} : Ni, C, N, Mn, Co and Cu. In most cases, the elemental groupings found by the FNN-1999 model are identical to the groupings that have been suggested in the literature over the years. The few exceptions are Si, Cu and V, which are discussed below.

The neural network calculations indicate that Si changes from a ferrite stabilizer to a weak austenite stabilizer at higher concentrations. When included in traditional constitution diagrams, Si is treated as a ferrite stabilizer. The reversal in behavior indicated by the FNN-1999 model and shown in Fig. 6 may explain the difficulty in identifying a statistically significant coefficient for Si in the WRC-1988 diagram (Ref. 13), the predecessor to the WRC-1992 diagram. As a result, Si was excluded from both of these diagrams.

Figure 6 indicates Cu is a very weak ferrite stabilizer for the austenitic stainless steel base composition. This is opposite to its role as an austenite stabilizer as identified in the WRC-1992 diagram. However, it should be noted the magnitude of the effect of Cu for the austenitic stainless steel base composition, as calculated by the FNN-1999 model, is very small. A change in Cu content from 0 to 0.6 results in an increase in FN of only 0.5, which is negligible. As shown later, for a different,

duplex stainless steel base composition, the effect of Cu is reversed and conforms with the behavior described in the WRC-1992 diagram. It is noteworthy that the Cu coefficient included in the WRC-1992 diagram was added after the additional data for duplex stainless steel test compositions was included.

The behavior of V as an austenite stabilizer is quite surprising and counterintuitive. One might expect V to tie up C and N, strong austenitizers and, by reducing their role, V would effectively be a ferrite stabilizer. However, the FNN-1999 results show this is not the case, at least for the austenitic stainless steel base composition that was considered. An attempt was made to examine the actual experimental data to see if this predicted behavior was justified by the experimental measurements. The nature of the database was such that a direct comparison of different V levels, with all other elemental additions held constant, was not possible. However, comparisons of the experimental data for nearly identical compositions except for V (V varied from 0 to 0.12) did indeed show a small austenite stabilizing effect of V, although the effect was quite small and may well be within the experimental error. The comparison unambiguously showed V did not have a strong ferrite stabilizer effect for this base composition and for V additions up to 0.12. It may be concluded the FNN-1999 model accurately

reflected the data it was trained on. Using computational thermodynamics (Ref. 14), calculations of the vertical section of the multicomponent phase diagram for the austenitic stainless steel base composition were made to examine the effect of vanadium content (0 to 0.3 wt-%) on the phase stability. These calculations showed that for the relatively low C and N levels of the base composition (0.08 and 0.01, respectively), vanadium carbonitride formation was not expected. These results indicate that the intuition-based interactions between vanadium and carbon and/or nitrogen do not take place for this composition, thus supporting the neural network results that show vanadium does not behave as a ferrite stabilizer. Predictions of unexpected behavior such as the effect of vanadium could be readily examined by producing new data specifically aimed at this base composition. Retraining the neural network on the new data could be readily accomplished if it were found the new data exhibited different trends

The neural network FN calculations as a function of composition can be evaluated even further if the average slopes of the curves in Fig. 6 are normalized to the slopes of either Cr or Ni. In this way, a quantity corresponding to the coefficients in the Cr_{eq} and Ni_{eq} expressions can be obtained. The results of these calculations are listed in Table 7. The number of expressions in the literature for the

Cr_{eq} and Ni_{eq} are too numerous to compare with the results in Table 7. However, it can be said the values in Table 7 are roughly comparable to the proposed coefficients in the literature (except for Si, Cu and V, as discussed above). In particular, the values for the Mo, Nb, C and N normalized slopes are of the same magnitude as the coefficients in the WRC-1992 constitution diagram (Ref. 5).

It is very instructive, and quite illuminating, to examine the individual element effects when the base composition is drastically different. Once again, a severe limitation of the most widely used constitution diagrams is that the Cr_{eq} and Ni_{eq} coefficients do not change as a function of the overall alloy composition. By doing the same analysis as above, and calculating the FN as a function of concentration but using a different base composition, the FNN-1999 model can provide valuable information as to how the elemental effects may change with base alloy composition. For comparison with the results in Fig. 6, a typical duplex stainless steel composition was chosen as a second starting composition. The composition was 66.77 Fe-22 Cr-5 Ni-3 Mo-2 Mn-1 Si-0.03 C-0.2 N. As was done earlier, the individual element concentrations were varied one at a time and the Fe level was adjusted accordingly. The range in compositions is listed in Table 8. The results of the calculations are shown in Fig. 7. As in Fig. 6, when the concen-

Table 7 — Average Slopes of Calculated FN (Using the FNN-1999 Model) vs. Concentration, and Normalized to the Slopes for Cr or Ni to Obtain Comparable Cr_{eq} or Ni_{eq} Coefficients

	Cr	Ti ^(a)	Mo	Nb	Cu	Ni ^(a)	V ^(a)	C	N	Mn	Co	Si ^(b)
Average slope	+3.6	+29.6	+5.0	+2.2	+0.8	-2.8	-17.6	-52.9	-48.3	-0.2	-2.1	—
Slope ÷ Cr slope	1	8.2	1.4	0.6	0.2	1	6.3	18.9	17.3	0.1	0.8	
Slope ÷ Ni slope						1	6.3	18.9	17.3	0.1	0.8	

Base composition is that of a typical austenitic stainless steel.

(a) The slope for Ti, Ni and V was not constant; an approximate value is given.

(b) The slope for Si varies from positive to negative and therefore a meaningful average slope could not be calculated.

Table 8 — Composition Ranges around a Starting Duplex Stainless Steel Composition for Which FN Was Calculated as a Function of Concentration Using the FNN-1999 Model

	C	Cr	Ni	Mo	N	Mn	Si	Cu	Ti	Nb	V	Co
Start	0.03	22	5	3	0.2	2	1	0	0	0	0	0
Min.	0.01	20	3	1	0.1	1	0.4	0.0	0.0	0.0	0.0	0.0
Max.	0.05	24	7	5	0.3	3	1.6	1.2	0.3	0.3	0.3	0.3

Table 9 — Average Slopes of Calculated FN (Using the FNN-1999 Model) vs. Concentration, and Normalized to the Slopes for Cr or Ni to Obtain Comparable Cr_{eq} or Ni_{eq} coefficients

	Cr	Ti	Mo	Nb	Si	V	Co	Ni	C	N	Mn	Cu
Average slope	+9.7	+122.8	+10.9	+3.1	+16.7	+106.4	+37.4	-16.9	-77.3	-197.1	-5.2	-9.0
Slope ÷ Cr slope	1	12.6	1.1	0.3	1.7	11.0	3.9					
Slope ÷ Ni slope								1	4.6	11.7	0.3	0.5

Base composition is that of a typical duplex stainless steel.

tration of only one element was varied (with the Fe concentration adjusted accordingly), all other element concentrations were held constant at the base metal value. The effect of concentration on FN for several elements is quite different from the behavior shown in Fig. 6. The effect of V is the opposite of what was seen before; V changes from a weak austenite stabilizer to a very strong ferrite stabilizer. Just the opposite holds for Cu; it changes from a weak ferrite stabilizer for an austenitic stainless steel base composition to an austenite stabilizer for a duplex steel base composition. The latter behavior is the same as indicated in the WRC-1992 diagram. Increasing Si concentration leads to a steady increase in FN, without the reversal seen in Fig. 6.

The slopes in Fig. 7 as well as the normalized values (with respect to the Cr or Ni slopes) are listed in Table 9. It is interesting to compare the potency of Cr and Ni for the two base compositions. Examination of the average slopes for these two elements in Tables 7 and 9 shows that Cr is a stronger ferrite stabilizer (steeper slope) and Ni is a stronger austenite stabilizer for the duplex stainless steel base composition. The values of the normalized slopes in Table 9 are also very different from those in Table 7 for many elements. This is a direct indication of a change in behavior when the base composition is changed from that of an austenitic stainless steel alloy to a duplex steel. The effect of C is diminished considerably. On the other hand, the influence of Ti and Co is enhanced. The effects of Mo, Nb and Mn are relatively unchanged.

Additional Comments

The use of neural networks for predicting Ferrite Number has an additional, potentially important advantage in that, in theory, process variables can be included as well as composition as inputs to the model. For example, many studies have shown that at high cooling rates prevalent during laser beam or electron beam welding, the residual ferrite content can be significantly different than that found for the same alloy under typical arc welding conditions (Refs. 15–21). The dramatic changes in ferrite content are often attributable to a change in the solidification mode so that an alloy that solidifies in the primary ferrite mode under near-equilibrium conditions can change to primary austenite solidification when rapidly cooled. In addition, rapid cooling after solidification will affect the solid-state transformation kinetics. In theory, this additional factor that influences Ferrite Number can be incor-

porated into a neural network model. Such an enhancement is planned for future work. Furthermore, if the training data set included data on the specific arc welding technique, in addition to the information on composition and FN, then the effect of arc welding process on the final FN could be included as well. This was not done in the present case since this additional information on arc welding process was not available.

The FNN-1999 model cannot be condensed into a simple pictorial form such as the WRC-1992 diagram. However, as shown in Figs. 6 and 7, important information on the influence of individual elements on the FN can be readily calculated. The neural network is especially easy to use in these types of calculations since the entire neural network can be easily converted into a spread sheet format. These types of calculations can yield even more useful information than the pictorial constitution diagram since the changing influence of various elements can be identified directly. For the interested reader, the FNN-1999 model is available over the Internet and sample calculations can be made. The neural network can be accessed at the following Web site: <http://engm01.ms.ornl.gov>.

Finally, it is interesting to speculate on other potential applications of neural network models beyond simply Ferrite Number prediction. In many cases, Ferrite Number prediction is not an end in itself. Ultimately, Ferrite Number prediction is a means for estimating an alloy's susceptibility to weld cracking or its mechanical properties, including its corrosion resistance. In this regard, it may be possible to use neural networks to directly correlate composition with these properties and bypass the intermediate Ferrite Number stage completely. Neural networks are ideally suited for such applications. Several neural network models have already been developed to predict weld alloy properties (Refs. 22, 23). The largest impediment for using neural network models to predict properties of stainless steels directly is the availability of a sufficiently complete database. If such a database were available, development of the required neural network models could easily follow and the need for constitution diagrams and Ferrite Number prediction could be eliminated altogether.

Conclusions

A neural network model, identified as FNN-1999, was developed to relate residual ferrite content in arc welds to alloy composition. Details of the neural network development are presented in

Part 1. The model uses the concentrations of thirteen elements (C, Cr, Ni, Mo, N, Mn, Si, Fe, Cu, Ti, Nb, V and Co) and shows a significant improvement in FN prediction accuracy compared to an earlier neural network model that considered the concentrations of only eight elements. It is also shown that the fitting error for the FNN-1999 model is 40% less than that for the WRC-1992 constitution diagram. In addition, the FNN-1999 model has the ability to account for significant variations in the influence of individual alloying additions as a function of overall alloy concentration. It is shown that such variations in the effect of alloying additions can be significant. For some alloying additions, the basic nature of their influence, in terms of the element behaving as an austenite stabilizer or ferrite stabilizer, was found to be reversed when the base composition was changed. The new FNN-1999 model provides a simple and quick means for predicting Ferrite Number in arc welds with a substantial improvement in the accuracy of the prediction compared to other models that are currently available.

Acknowledgments

This research was sponsored by the Division of Materials Sciences, U.S. Department of Energy, under contract DE-AC05-96OR22464 with Lockheed Martin Energy Research Corp. The authors wish to acknowledge the help of C. McCowan, National Institute of Standards and Technology, Boulder, Colo., for providing the supplemental data set in electronic form and F. Lake, ESAB Welding and Cutting Products, Inc., for providing the software for calculating the WRC-1992 Ferrite Number as a function of composition. The authors would also like to thank S. S. Babu for making the FNN-1999 model available on the World Wide Web. Finally, the authors wish to acknowledge S. S. Babu, D. J. Kotecki and T. A. Siewert for reviewing the manuscript and providing helpful comments.

References

1. Vitek, J. M., Iskander, Y. S., and Oblow, E. M. 2000. Improved ferrite number prediction in stainless steel arc welds using neural networks — part 1: neural network development. *Welding Journal* 79(2): 33-s to 40-s.
2. Kotecki, D. J. 1986. Ferrite control in duplex stainless steel weld metal. *Welding Journal* 65(10): 273-s to 278-s.
3. Kotecki, D. J. 1989. Heat treatment of duplex stainless steel weld metal. *Welding Journal* 68(11): 431-s to 441-s.
4. McCowan, C. N., Siewert, T. A., and Olson, D. L. 1989. Stainless steel weld metal: prediction of ferrite content. *WRC Bulletin* 342: 1–36.

5. Kotecki, D. J., and Siewert, T. A. 1992. WRC-1992 constitution diagram for stainless steel weld metals: a modification of the WRC-1988 diagram. *Welding Journal* 71(5): 171-s to 178-s.
6. Kotecki, D. J. 1988. Verification of the NBS-CSM Ferrite Diagram. International Institute of Welding Document II-C-834-88.
7. Ornig, H. 1988. *Proceedings International Institute of Welding 41st Annual Assembly and International Conference*, Vienna, July.
8. Babu, S. S., Vitek, J. M., Iskander, Y. S., and David, S. A. 1997. New model for prediction of ferrite number of stainless steel welds. *Science and Technology of Welding and Joining* 2(6): 279-285.
9. Vitek, J. M., Iskander, Y. S., Oblow, E. M., Babu, S. S., and David, S. A. 1999. Neural network model for predicting ferrite number in stainless steel welds. *Trends in Welding Research*, eds. J. M. Vitek, S. A. David, J. A. Johnson, H. B. Smarrt and T. DebRoy, pp. 119-124. ASM International, Materials Park, Ohio.
10. Lake, F. B. 1997. ESAB Welding and Cutting Products, Hanover, Pa.
11. Lake, F. B. 1998. Expansion of the WRC-1992 ferrite diagram and nitrogen prediction. Abstracts of Papers, 1998 AWS Convention, Detroit, pp. 214-215.
12. Olson, D. L. 1985. Prediction of austenitic weld metal microstructure and properties. *Welding Journal* 64(10): 281-s to 295-s.
13. Siewert, T. A., McCowan, C. N., and Olson, D. L. 1988. Ferrite number prediction to 100 FN in stainless steel weld metal. *Welding Journal* 67(12): 289-s to 298-s.
14. Sundman, B., Jansson, B., and Andersson, J.-O. 1985. The ThermoCalc databank system. *Calphad* 9: 153 to 190.
15. Vitek, J. M., DasGupta, A., and David, S. A. 1983. Microstructural modification of austenitic stainless steels by rapid solidification. *Metallurgical Transactions A* 14A: 1833-1841.
16. Katayama, S., and Matsunawa, A. 1984. Solidification microstructure of laser welded stainless steels. *Proc. of ICALCO 84*, Boston, Mass., 44: 60-67.
17. David, S. A., Vitek, J. M., and Hebble, T. L. 1987. Effect of rapid solidification on stainless steel weld metal microstructures and its implications on the Schaeffler diagram. *Welding Journal* 66: 289-s to 300-s.
18. Bobadilla, M., Lacaze, J., and Lesoult, G. 1988. Influence des conditions de solidification sur le déroulement de la solidification des aciers inoxydables austénitiques. *Journal of Crystal Growth* 89: 531-544.
19. Elmer, J. W., Allen, S. M., and Eagar, T. W. 1989. Microstructural development during solidification of stainless steel alloys. *Metallurgical Transactions A* 20A: 2117-2131.
20. Lippold, J. C. 1994. Solidification behavior and cracking susceptibility of pulsed laser welds in austenitic stainless steels. *Welding Journal* 73(6): 129-s to 139-s.
21. Koseki, T. and Flemings, M. C. 1997. Solidification of undercooled Fe-Cr-Ni alloys: part III. Phase selection in chill casting. *Metallurgical and Materials Transactions A* 28A: 2385-2395.
22. Chan, B., Bibby, M., and Holtz, N. 1995. Predicting HAZ hardness with artificial neural networks. *Canadian Metallurgical Quarterly* 34: 353-356.
23. Cool, T., Bhadeshia, H. K. D. H., and MacKay, D. J. C. 1997. The yield and ultimate tensile strength of steel welds. *Materials Science and Engineering A* 223: 186-200.

Papers Needed For ASTM Symposium on Outdoor and Indoor Atmospheric Corrosion

Papers are invited for a Symposium on Outdoor and Indoor Atmospheric Corrosion sponsored by ASTM Committee G-1 on Corrosion of Metals. The symposium will be held May 8-9, 2001, in Phoenix, Ariz., in conjunction with the Committee's May 9-11, 2001, standards development meetings.

This symposium focuses on predicting the performance of materials in the atmosphere, both outdoors and indoors. Its purposes are to record information on the corrosion behavior of traditional materials and the newer alloys and coatings, describe atmospheric corrosion mechanisms and rates and effect of environmental variables such as pollutants and wetness, discuss systems of classification of the corrosivity of atmospheres, and describe how various tests can be used to simulate and predict atmospheric corrosion.

Sessions on outdoor atmospheric corrosion will deal with the performance of such metals as ordinary steels; weathering steels; stainless steels; alloys of aluminum, copper, nickel and titanium; and metallic coatings in industrial, rural, marine and tropical environments. The effects of environmental variables on corrosion performance will be examined, as well as data on defining and controlling the effects of corrosion product runoff on the environment.

The sessions on indoor atmospheric corrosion will focus on accelerated testing to predict the long-term behavior of materials. These include electrical and electronic systems, architectural and building materials, appliances, household appurtenances and others. Among the subjects of discussion are mechanisms unique to indoor exposure, characterization and classification of indoor environments with respect to corrosivity, and correlation of corrosion tests with service life.

Prospective authors are requested to submit a title, a 250-300 word preliminary abstract and an ASTM paper submittal form by May 8 to Dorothy A. Fitzpatrick, Symposia Operations, ASTM, 100 Barr Harbor Dr., W. Conshohocken, PA 19428-2959 (610/832-9677). Paper submittal forms are available from Fitzpatrick or from the symposium chairman. Do not send abstracts by fax or e-mail.

ASTM anticipates a Special Technical Publication (STP) based on the symposium proceedings. The symposium chairman will notify you by July 8 of your paper's acceptability for presentation. All accepted manuscripts to be peer reviewed for the STP will be due at ASTM by March 8, 2001.

More information is available from Symposium Chairman Herbert E. Townsend, Ph.D., P.E., Bethlehem Steel Corp., Homer Research Laboratories, Bethlehem, PA 18016 (610/694-6674; fax: 610/694-1739; e-mail: rheto@bsco.com); or Robert Baboian, Ph.D., P.E., RB Corrosion Service, 84 Ruff Stone Road, Greenville, RI 02828 (401/949-5398; fax: 401/949-1661; e-mail: rbaboian@aol.com).